ELECTROMAGNETIC SOUNDING OF BOTTOM CREVASSES ON THE ROSS ICE SHELF, ANTARCTICA*

By Kenneth C. Jezek, Charles R. Bentley,

(Geophysical and Polar Research Center, Department of Geology and Geophysics, University of Wisconsin—Madison, Madison, Wisconsin 53706, U.S.A.)

and John W. Clough

(Ross Ice Shelf Project, 135 Bancroft Hall, University of Nebraska—Lincoln, Lincoln, Nebraska 68588, U.S.A.)

Abstract. During the 1976–77 season of the Ross Ice Shelf Geophysical and Glaciological Survey, a series of vertical electromagnetic sounding profiles of subsurface features was completed at station J-9. The survey comprised three five-kilometer north-west–south-east profiles separated by one kilometer and six two-kilometer north-east–south-west profiles, and was carried out on the surface using 35 MHz and 50 MHz radar systems. Folded-dipole antennae were used and oriented to detect reflectors both along and perpendicular to the profile path. This was done to facilitate the interpretation of the data, which indicated a complex system of bottom crevasses. Measurements of the positions, heights, and shapes of these crevasses showed at least two sets of crevasses varying in both strike and size. The larger crevasses, about 120 m high and oriented more or less normal to the flow direction, are probably associated with the movement of ice stream B across the grounding line between the West Antarctic ice sheet and the Ross Ice Shelf. A satisfactory explanation for the secondary set of crevasses, about 60 m high and forming an angle of $60° \pm 10°$ with the first set, has not yet been found.

Résumé. *Sondages électromagnétiques verticaux dans le Ross Ice Shelf, Antarctique, en un point montrant des crevasses de fond.* Au cours de la saison 1976–77 de l'Expédition glaciologique et géophysique du Ross Ice Shelf, on a mené à bien à la station J-9 une série de sondages électromagnétiques verticaux pour explorer la zone sous la surface. Le programme comprenait trois profils de cinq kilometres de direction Nord-Ouest Sud-Est espacés d'un kilometre et six profils Nord-Est Sud-Ouest de 2 km, qui ont été exécutés depuis la surface avec des radars de 35 MHz et de 50 MHz. On a utilisé des antennes dipoles repliées et orientées de manière à détecter les réflecteurs aussi bien perpendiculaires que parallèles à la direction des profils. Ceci afin de faciliter l'interprétation des résultats qui indiquent un système complexe de crevasses de fond. Les mesures des positions hauteur et forme de ces crevasses ont montré au moins deux catégories de crevasses différentes à la fois par la direction et par la dimension. Les plus grandes crevasses d'environ 120 m de haut et orientées plus ou moins perpendiculairement à la direction de l'écoulement sont probablement associées au mouvement du courant de glace B à travers la ligne au sol séparant la calotte Ouest Antarctique et la Ross Ice Shelf. On n'a pas encore trouvé une explication satisfaisante pour la seconde catégorie de crevasses qui ont environ 60 m de haut et forment un angle de $60° \pm 10°$ avec les crevasses du premier type.

Zusammenfassung. *Vertikale elektromagnetische Tiefenmessungen auf dem Ross Ice Shelf, Antarktika, an einer Stelle mit Spalten am Untergrund.* Während der Sommerkampagne 1976–77 des Ross Ice Shelf Geophysical and Glaciological Survey wurde eine Serie von elektromagnetischen Tiefenprofilen zur Sondierung von Untergrundserscheinungen bei Station J-9 aufgenommen. Die Aufnahme umfasste drei, 5 km lange, NW–SE-gerichtete Profile im Abstand von je 1 km und sechs, 2 km lange Profile von NE nach SW; sie wurde an der Oberfläche mit 35 MHz- und 50 MHz-Radargeräten durchgeführt. Es wurden gekreuzte Dipolantennen benutzt und so ausgerichtet, dass Reflexionen sowohl in Profilrichtung wie senkrecht dazu empfangen werden konnten. Dies sollte die Interpretation der Daten erleichtern, die ein komplexes System von Spalten an der Unterseite vermuten liessen. Die Bestimmung der Lage, der Höhe und der Form dieser Spalten ergab zumindest 2 Systeme von Spalten, die sich sowohl in der Richtung wie in der Grösse unterscheiden. Die grösseren Spalten, die 120 m hoch und mehr oder weniger genau senkrecht zur Fliessrichtung orientiert sind, sind vermutlich mit der Bewegung des Eisstroms B verbunden, der die Aufsetzlinie zwischen dem westantarktischen Eis und dem Ross Ice Shelf überquert. Für das System sekundärer Spalten, die 60 m hoch sind und mit dem ersten System einen Winkel von $60° \pm 10°$ bilden, wurde noch keine befriedigende Erklärung gefunden.

Introduction

During the 1976–77 field season of the Ross Ice Shelf Geophysical and Glaciological Survey (RIGGS), radar profiling of the ice was carried out at station J-9 (Fig. 1) where an earlier survey (Clough and others, 1975) had revealed a complex arrangement of crevasses extending into the lower part of the ice shelf. These features, probably frozen wedges of salty

ice, are presumably not forming or growing at J-9, but serve as evidence of large stresses acting on the ice somewhere up-stream.

The data collected by Clough and others (1975) showed at least two large crevasses intersecting the traverse lines, and other features that were uninterpretable at that time. The more extensive grid that was completed in the 1976–77 season has yielded a more accurate determination of the position of the crevasses, as well as details about their heights and shapes.
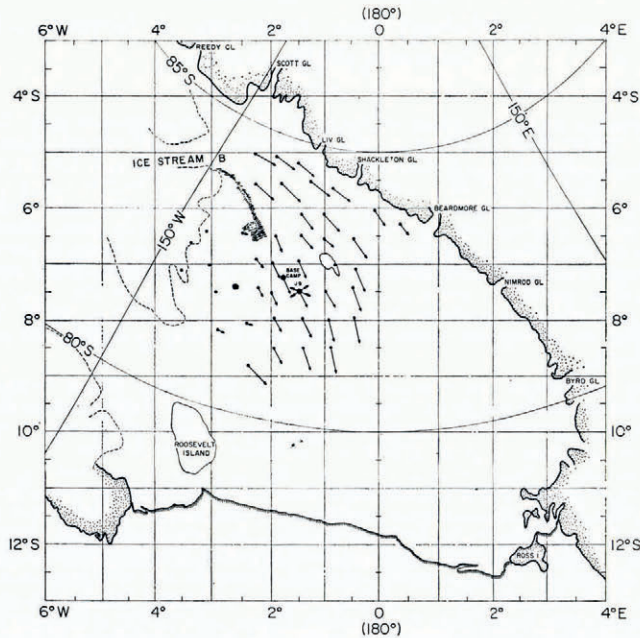
Fig. 1. *Map of the Ross Ice Shelf. The arrows are velocity vectors (after Thomas, 1976), surface crevasses (modified from the U.S. Geological Survey map of the Ross Ice Shelf) are also shown.*

EXPERIMENT

The rectangular grid surveyed at J-9 comprised three five-kilometer lines, one kilometer apart oriented north-west–south-east (magnetic north–south). This grid overlies the earlier survey lines (Clough and others, 1975), which consisted of the A, C, and D lines and a portion of the B line (Fig. 2). Profiling was carried out in both the north-west–south-east and north-east–south-west directions. (Some diagonal lines were also profiled, but the actual route taken between flagged points was not well determined.) Distances were measured with an odometer wheel and flags were placed every 500 m. Errors in measured distances should not exceed one per cent.

Scott Polar Research Institute Mark II radar transmitters and receivers (Evans and Smith, 1969) operating at 35 and 50 MHz were used to sound the ice. Two folded dipoles acted as antennae and were separated by 30 m in order to decrease receiver saturation by the air wave. Although the beam pattern of the folded dipoles is broad (Clough, unpublished), reflections from the front and rear, and to the sides, can be emphasized by orienting both antennae either perpendicular (antennae parallel) or parallel (antennae collinear) to the traverse line, respectively. Both antennae configurations were used to collect the data.
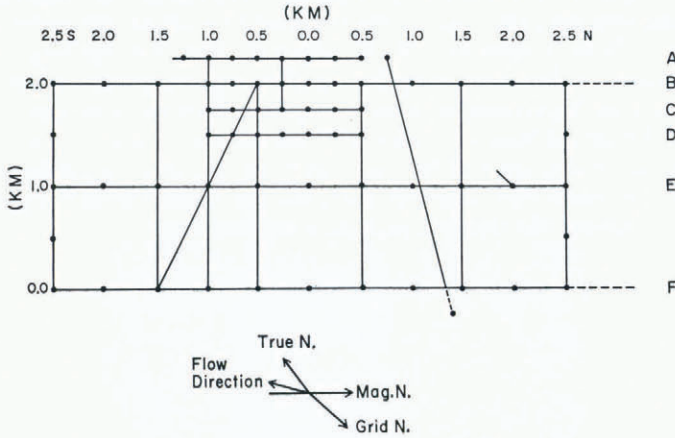
Fig. 2. *Profile lines at J-9. The dots indicate flagged points. The A, C, D, and adjacent portion of the B lines were surveyed during the 1974–75 season.*
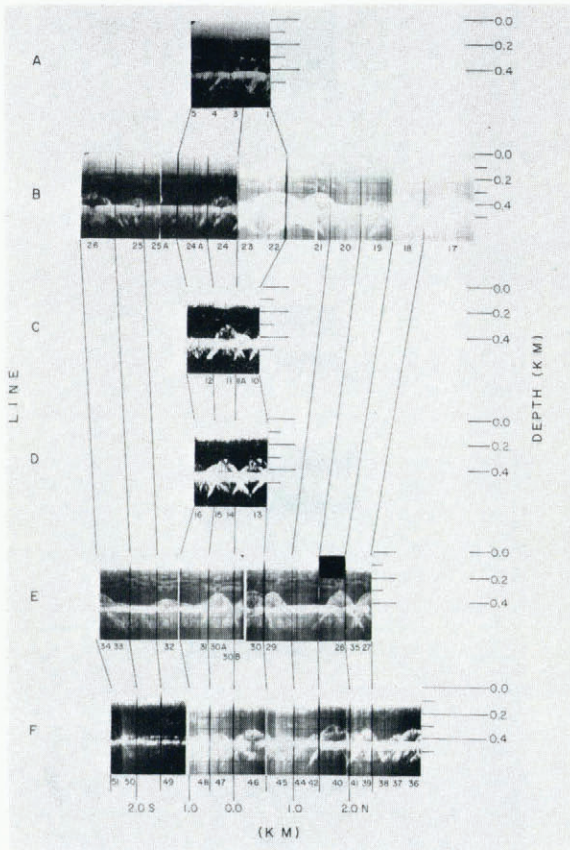
Fig. 3. *North-west–south-east data collected with antennae parallel. The numbers are used to identify reflection hyperbolae and are positioned approximately below the vertex. The dark lines between profiles connect corresponding flagged positions on each profile. Profile lengths vary due to different sweep and vehicle speeds.*

Profiles of the ice were constructed by intensity-modulating the oscilloscope trace of the received signals and sweeping the trace across Polaroid film whilst the system was being towed across the surface. Figure 3 shows the data collected along the north-west–south-east lines with antennae parallel. (The data along the A, C, and D lines were collected in the earlier survey.) The numerous hyperbolic features represent reflections from linear reflectors which we interpret to be the tops of bottom crevasses. Two sets of crevasses are present. One set (I), represented by the narrowest hyperbolae (such as 3, 24, 11, and 14), strikes nearly perpendicular) to the traverse path; the other set (II), having much broader hyperbolae (such as 33, 32, 12, and 19), crosses the traverse path at a shallow angle.
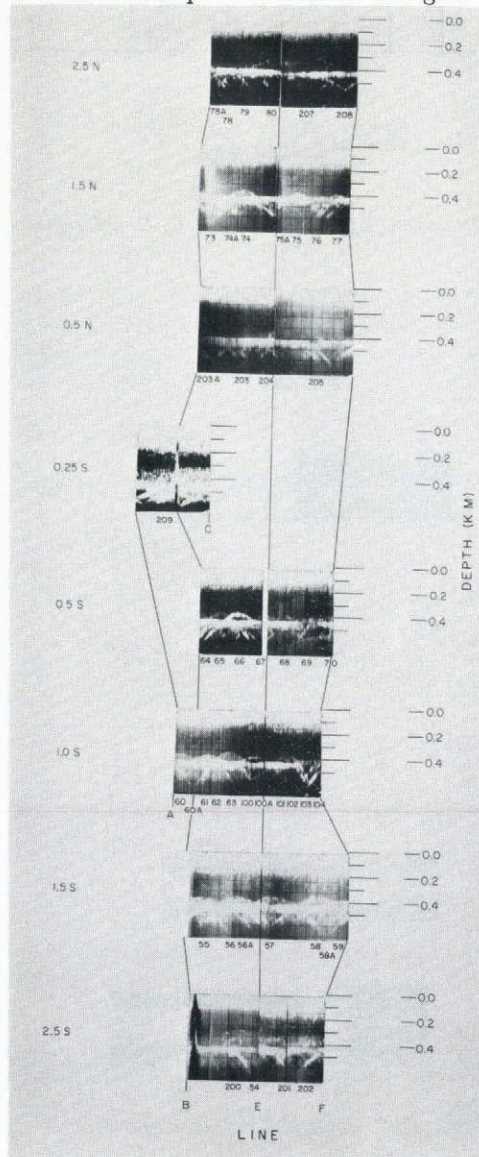
Fig. 4. *North-east–south-west data collected with antennae parallel. The numbers are used to identify features and are positioned approximately below the vertex. The dark lines between profiles connect corresponding flagged positions on each profile. Profile lengths vary due to different sweep and vehicle speeds.*

Figure 4 shows the data collected along north-east–south-west traverses, also with antennae parallel. Again there are many hyperbolae, but with smaller heights than many of those in Figure 3. There are also some long features at a depth which is nearly constant (209, for example), which are due to reflectors that run nearly parallel to the traverse path. Data with antennae collinear, collected only along the B, E, and F lines, are shown in Figure 5.
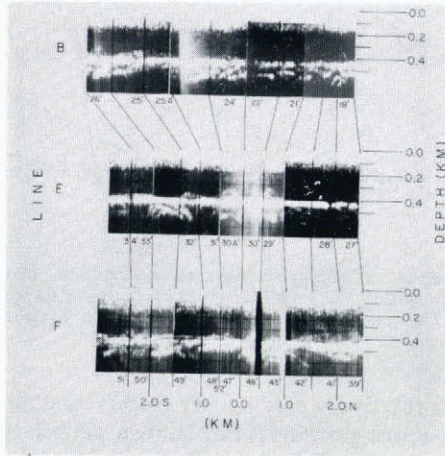
Fig. 5. *North-west–south-east data collected with antennae collinear. The numbers are used to identify features and, except for 52′, correspond to the numbers in Figure 3. Primes are used to differentiate a feature observed on the collinear data from the same feature on the parallel data. The dark lines between profiles connect corresponding flagged positions on each profile. Profile lengths vary due to different sweep and vehicle speeds.*

RESULTS

Assuming that the apex of a crevasse can be represented by a horizontal straight line, the vertex of the associated reflection hyperbola is found at the intersection of the traverse line and the crevasse, and the corresponding reflection time gives the depth to the crevasse. The vertices of the hyperbolae are shown in Figure 6 (together with the identifying numbers from Figs 3, 4, and 5). Figure 7 shows the height of each crevasse above the ice–water boundary. Errors in travel-time measurements should not exceed ± 0.1 μs^{-1}, leading to crevasse-height errors of about ± 10 m.
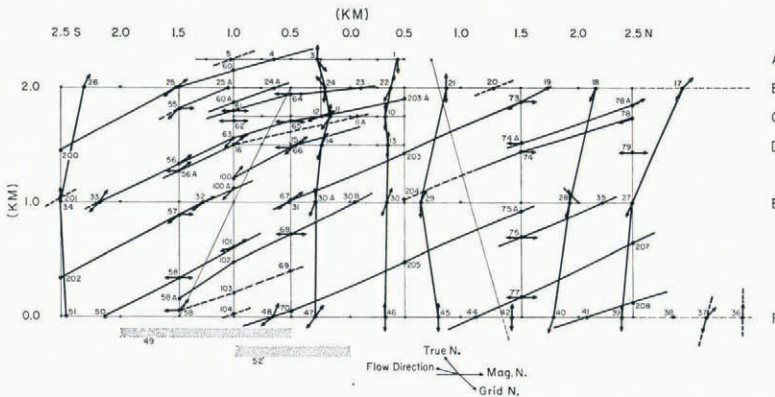
Fig. 6. *Crevasse map with identifying numbers corresponding to those on Figures 3, 4, and 5. The heavy solid lines represent crevasses. Dashed lines indicate possible crevasse locations, although the evidence may be weak. The stippled bands at the bottom of the map represent poorly-defined features that may run parallel to the F line. Their position below the F line is arbitrary. The arrows are strike directions calculated from the shapes of the reflection hyperbolae.*
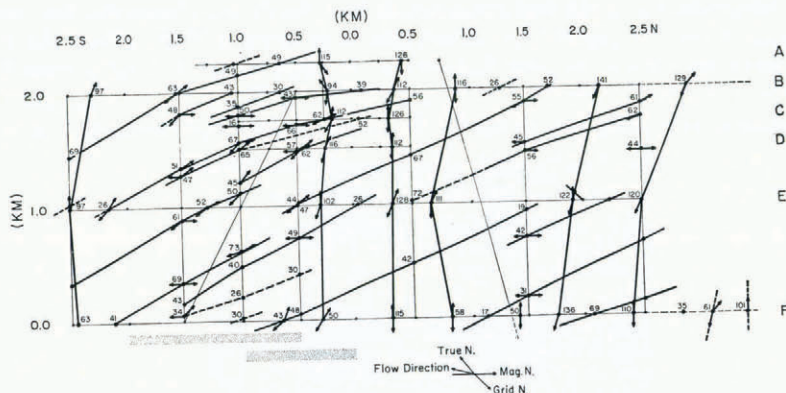
Fig. 7. Crevasse map showing crevasses heights. The heavy solid lines represent crevasses. Dashed lines indicate possible crevasse locations although the evidence may be weak. The stippled bands at the bottom of the map represent poorly defined features that may run parallel to the F line. Their position below the F line is arbitrary. The arrows are strike directions calculated from the shapes of the reflection hyperbolae.

With this information it is a relatively easy matter to correlate the higher crevasses of set I from line to line. For instance, 1 and 3 on the A line show a pattern that is easily traced to the E line and, with some confidence, to the F line. Similarly, the large hyperbolae 26, 34, and 51, are certainly related, as are the large hyperbolae at the north-west end of the section. There is little ambiguity in the position and trend of this set of crevasses.

Mapping the crevasses of set II was more difficult as few of these crevasses display distinctive patterns that facilitate correlation between traverse lines. Furthermore, the crevasses are more numerous than those of set I, and, it turns out, not all of them are continuous across the grid. Hence the same grid-line spacing that yielded more than enough information about the crevasses of set I is only marginally adequate for set II.

However, additional information about the strike of a crevasse may be obtained from examination of the shape of the reflection hyperbolae. Assuming that the crevasse depth h is constant over the sensing range of the radar, the reflection time T is given by

$$T^2v^2 = 4x^2 \sin^2\theta + 4h^2,$$

where x is the horizontal distance to the intersection of the traverse path and the crevasse, θ is the angle between them, and v is the wave speed. As θ decreases, the hyperbola becomes broader until at $0°$ the reflection time becomes constant. θ is determined by plotting T^2 against x^2; the slope of a straight-line fit to these points gives $\sin^2\theta$, since v is known. (The velocity used for the depth calculations was 173 m μs^{-1}, about 3 m μs^{-1} less than the measured velocity (Jezek and others, 1978), and was selected because of the uncertainties in the travel times for antennae separations of less than 80 m.) This calculation was performed on all the reasonably well-defined reflection hyperbolae. A sample set of T^2 against x^2 plots, including crevasses from both sets, is shown in Figure 8. The right and left sides of each hyperbola are taken as separate sets of data. The results of these calculations are shown as the arrows associated with the crevasse locations in Figures 6 and 7.

Because the radar does not differentiate between signals arriving from opposite sides, the strike arrows in Figures 6 and 7 represent only one of two arrows that are symmetric about the traverse line. Initially, both arrows were plotted but, through the process of correlation, it became possible to eliminate one set.

The distribution of crevasse crossings, heights, and strikes strongly suggests the pattern of crevasses mapped in Figures 6 and 7. The collinear data of Figure 5 also support this interpretation. The crevasses of set I appear as hyperbolae, whereas those of set II appear as sloping
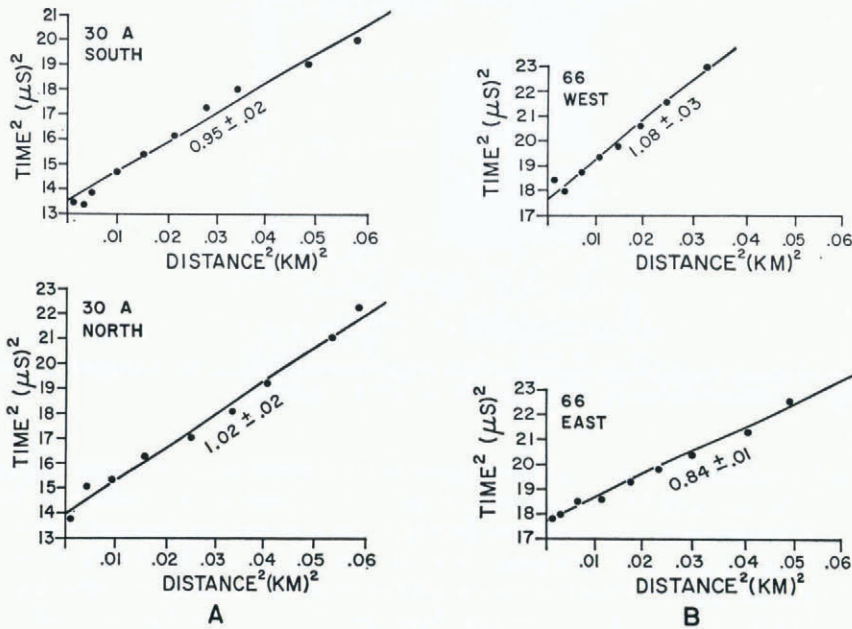
Fig. 8. *T² against x² plots from which strike arrows are calculated. The number below the line fit to each set of data is the calculated value for sin θ. Reasons why this value may be greater than one are discussed in the text. A shows a sample crevasse from set I, B a sample crevasse from set II.*

lines (i.e. single hyperbolic limbs), showing crevasses subparallel to the traverse line. In addition, the collinear data tend to suggest a pair of reflectors parallel to the F line (49 and 52). These two features have been placed an arbitrary distance away from the F line since their heights are unknown, and to the south-west (grid) since there are no obvious reflections on the north-east–south-west traverse lines with which they could be well correlated.

The reflection data yield, together with positions and heights, a measure of the basal width of the bottom crevasses. Just as there is a reflection hyperbola originating at the top of a crevasse, hyperbolae also originate at the intersection of the crevasse with the ice–water boundary. These lower hyperbolae are clearly seen at 28 in Figure 9, and on many of the other crevasses. Initially, it was assumed that the bottom reflection represented a single hyperbola and that the crevasses were thin wedges, but in Figure 9, however, it can be seen that the lower reflections form two hyperbolae spatially separated by about 130 m. The downward-trending hyperbolic limbs yield the cusp-like features seen beneath many of the crevasses. Assuming that the lower edges of an intruding wedge are the reflectors responsible for the bottom hyperbolae, and that they are situated on the same horizontal plane, measurement of the separation of the reflection hyperbolae yields the basal width. In some instances, such as 28, the two vertices could be measured directly. In other cases, hyperbolae were fitted to the lower parts of the limbs to estimate the position of the vertex.

A number of the strike arrows in Figures 6 and 7 are perpendicular to the traverse line. Many of these actually represent calculations which produced a value for sin θ significantly greater than one—usually only on one limb of the hyperbola (Fig. 8). These values could be caused by the migration of the reflection point along a dipping crevasse, or, possibly, up the sides of a concave crevasse. These results might also occur if an incorrect value for the velocity was chosen. However, varying the velocity by ±3.0 m μs⁻¹ affects the values of sin θ greater than one by only ±0.02 and hence does not completely account for this anomalous result.
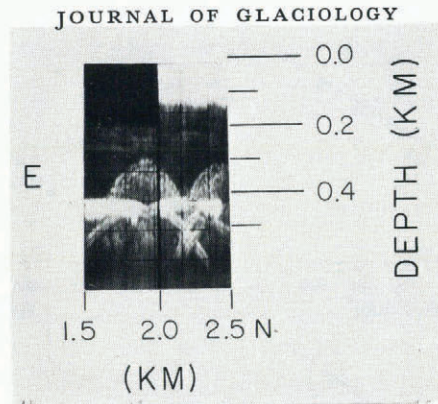
Fig. 9. Crevasse 28 showing two hyperbolae generated at the base of the crevasse (depth 0.42 km) and separated by about 130 m. The vertices are positioned horizontally at about 1.9° N. and 2.0° N., respectively.

Further, similar calculations on six of the hyperbola pairs generated at the intersections of the crevasses with the ice–water boundary showed the same trends as calculations on the corresponding upper hyperbolae. This suggests that the cause—at least on these six—is local curvature of the crevasse in the horizontal plane, such as the bend at 11 (Fig. 6). If we assume that the crevasse is bent, the reflections from the convex side will produce an apparent value of sin θ that will be not only higher than those from the concave side, but also can be greater than one—roughly consistent with our results.

The crevasses given by features 3, 24, 11, 14, and 30A were well enough delineated to be drawn in three dimensions. Figure 10 shows clearly that the larger bottom crevasses are not only deeper than most surface crevasses, but wider as well. Some of the upper hyperbolae appear not to be centered between the corresponding lower pair, suggesting an asymmetry in the crevasse cross-section, but the data were insufficiently accurate to describe any asymmetry quantitatively; accordingly, the crevasses in Figure 10 have been drawn symmetrically.
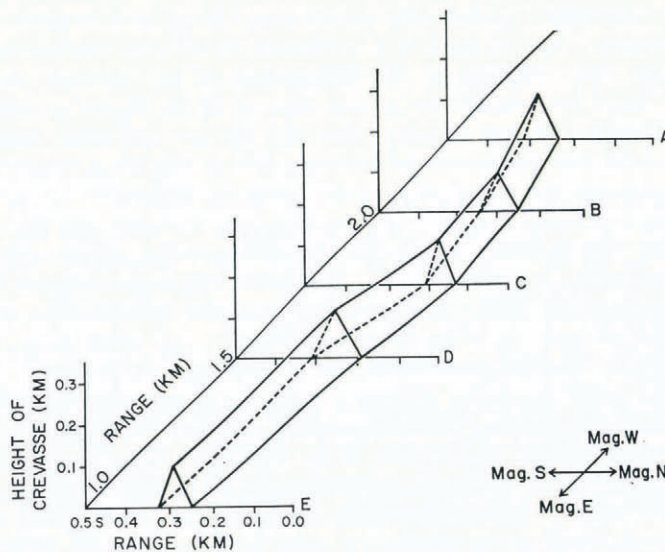
Fig. 10. A three-dimensional representation of the bottom crevasse defined by features 3, 24, 11; 14, and 30A.

Only one width measurement was possible on the crevasses of set II, probably due to their smaller size. The width of feature 56 was found to be 30 m. The error on all basal-width measurements is at least ± 10 m.

Because of the limited size of the survey area, no estimate of the length of any crevasse is possible. We can say that the set I crevasses extend at least 2.3 km and the set II crevasses at least 3 km.

DISCUSSION

Velocity vectors determined from satellite positioning and surface strain-rate measurements (Thomas, 1976) show that the ice containing the bottom crevasses originated in ice stream B (Fig. 1). Figure 1 also shows a region of surface crevasses that probably mark the lateral boundary of ice stream B (modified from the U.S. Geological Survey map of the Ross Ice Shelf using RIGGS airborne-radar data). The surface crevasses presumably represent a shear zone—the crevasses roughly conform to a pattern resulting from shear of the ice along the ice-stream margin.

Although the orientation of crevasses on the U.S. Geological Survey map may not be very accurate, there does seem to be agreement between the orientation of those surface crevasses and crevasse set I at J-9. Nye (1952) shows that, for a glacier subject to tensile stress both along and across the direction of flow (e.g. extending flow through a widening valley) together with shear stress from the constraining walls, the surface cracks that will develop have a pattern remarkably similar to the pattern we observe at J-9. If the crevasses at J-9 were formed in ice stream B under such a stress system, then the crevasses of set I represent those opening primarily due to shear and the crevasses of set II are those resulting from transverse tension. This model conforms with the observations by Clough (1974) of a single large set of bottom crevasses at the RIGGS 1973–74 Base Camp. At that location the absence of a second set of crevasses would, by Nye's model, imply smaller (or negative) transverse stresses, indicating that the ice now at Base Camp was nearer to the boundary walls of the ice stream, as is indeed the case (Fig. 1).

Whilst the Nye model gives a good qualitative description of the pattern of bottom crevasses, it is not clear how the shear stresses could produce the large, wide features of set I. For this reason, a second model that invokes tensile forces at the boundary between the grounded and floating ice, related to the Base Camp results by Holdsworth (1977), may be preferred. Cracks develop to relieve the tension and are kept open by tidal flexure, presumably deepening and widening the features. This is a good model to explain the set I crevasses, but it does not show how the second set of crevasses could form. A combination of both models may be necessary to cause the formation of crevasses at J-9.

CONCLUSIONS

A distinct pattern of bottom crevasses has been observed in the Ross Ice Shelf at station J-9. The crevasses form two sets striking towards each other at an angle of $60° \pm 10°$. The wider and larger crevasses, forming a set approximately normal to the flow direction, probably developed at or near the grounding line of ice stream B. The secondary set may result from the lateral spreading of the ice as it flows into the ice shelf from ice stream B.

ACKNOWLEDGEMENTS

REFERENCES

Clough, J. W. 1974. RISP radio-echo sounding. *Antarctic Journal of the United States*, Vol. 9, No. 4, p. 159.

Clough, J. W. Unpublished. Propagation of radio waves in the Antarctic ice sheet. [Ph.D. thesis, University of Wisconsin—Madison, 1974.]

Clough, J. W., *and others.* 1975. RISP drill site survey, [by] J. W. Clough, K. C. Jezek, and J. D. Robertson. *Antarctic Journal of the United States*, Vol. 10, No. 4, p. 148–49.

Evans, S., *and* Smith, B. M. E. 1969. A radio echo equipment for depth sounding in polar ice sheets. *Journal of Scientific Instruments (Journal of Physics, E)*, Ser. 2, Vol. 2, No. 2, p. 131–36.

Holdsworth, G. 1977. Tidal interaction with ice shelves. *Annales de Géophysique*, Tom. 33, Fasc. 1–2, p. 133–46.

Jezek, K. C., *and others.* 1978. Dielectric permittivity of glacier ice measured *in situ* by radar wide-angle reflection, by K. C. Jezek, J. W. Clough, C. R. Bentley, and S. Shabtaie. *Journal of Glaciology*, Vol. 21, No. 85, p. 315–29.

Nye, J. F. 1952. The mechanics of glacier flow. *Journal of Glaciology*, Vol. 2, No. 12, p. 82–93.

Thomas, R. H. 1976. Ice velocities on the Ross Ice Shelf. *Antarctic Journal of the United States*, Vol. 11, No. 4, p. 279–81.